Research Article

EASL EUROPEAN ASSOCIATION FOR THE STUDY OF THE LIVER | JOURNAL OF HEPATOLOGY

Serum metabolomics reveals γ-glutamyl dipeptides as biomarkers for discrimination among different forms of liver disease

Tomoyoshi Soga[1,*], Masahiro Sugimoto[1], Masashi Honma[2], Masayo Mori[1], Kaori Igarashi[1], Kasumi Kashikura[1], Satsuki Ikeda[1], Akiyoshi Hirayama[1], Takehito Yamamoto[2], Haruhiko Yoshida[3], Motoyuki Otsuka[3], Shoji Tsuji[4], Yutaka Yatomi[4], Tadayuki Sakuragawa[5], Hisayoshi Watanabe[6], Kouei Nihei[7], Takafumi Saito[6], Sumio Kawata[6], Hiroshi Suzuki[2], Masaru Tomita[1], Makoto Suematsu[5]

[1]*Institute for Advanced Biosciences, Keio University, Tsuruoka 997-0052, Japan;* [2]*Department of Pharmacy, The University of Tokyo Hospital, Hongo, Bunkyo-ku, Tokyo 113-8655, Japan;* [3]*Department of Gastroenterology, Faculty of Medicine, The University of Tokyo, Hongo, Bunkyo-ku, Tokyo 113-8655, Japan;* [4]*Department of Neurology, Division of Neuroscience, Graduate School of Medicine, The University of Tokyo, Hongo, Bunkyo-ku, Tokyo 113-8655, Japan;* [5]*Department of Biochemistry, JST ERATO Suematsu Gas Biology Project, School of Medicine, Keio University, Shinanomachi, Shinjuku-ku, Tokyo 160-8582, Japan;* [6]*Department of Gastroenterology, Yamagata University School of Medicine, Yamagata 990-9585, Japan;* [7]*Department of Surgery, Shonai Hospital, 4-20 Izumi-cho, Tsuruoka 997-8515, Japan*

Background & Aims: We applied a metabolome profiling approach to serum samples obtained from patients with different liver diseases, to discover noninvasive and reliable biomarkers for rapid-screening diagnosis of liver diseases.

Methods: Using capillary electrophoresis and liquid chromatography mass spectrometry, we analyzed low molecular weight metabolites in a total of 248 serum samples obtained from patients with nine types of liver disease and healthy controls.

Results: We found that γ-glutamyl dipeptides, which were biosynthesized through a reaction with γ-glutamylcysteine synthetase, were indicative of the production of reduced glutathione, and that measurement of their levels could distinguish among different liver diseases. Multiple logistic regression models facilitated the discrimination between specific and other liver diseases and yielded high areas under receiver-operating characteristic curves. The area under the curve values in training and independent validation data were 0.952 and 0.967 in healthy controls, 0.817 and 0.849 in drug-induced liver injury, 0.754 and 0.763 in asymptomatic hepatitis B virus infection, 0.820 and 0.762 in chronic hepatitis B, 0.972 and 0.895 in hepatitis C with persistently normal alanine transaminase, 0.917 and 0.707 in chronic hepatitis C, 0.803 and 0.993 in cirrhosis type C, and 0.762 and 0.803 in hepatocellular carcinoma, respectively. Several γ-glutamyl dipeptides also manifested potential for differentiating between nonalcoholic steatohepatitis and simple steatosis.

Conclusions: γ-Glutamyl dipeptides are novel biomarkers for liver diseases, and varying levels of individual or groups of these peptides have the power to discriminate among different forms of hepatic disease.

Keywords: γ-Glutamyl dipeptides; Metabolomics; Biomarker; Capillary electrophoresis mass spectrometry; Oxidative stress; Glutathione; Hepatocellular carcinoma; Nonalcoholic steatohepatitis; Hepatitis C virus.

Received 15 July 2010; received in revised form 17 January 2011; accepted 24 January 2011; available online 18 February 2011

* Corresponding author. Address: Institute for Advanced Biosciences, Keio University, 246-2 Mizukami, Kakuganji, Tsuruoka, Yamagata 997-0052, Japan. Tel.: +81 235 29 0528; fax: +81 0235 29 0574.

E-mail address: soga@sfc.keio.ac.jp (T. Soga).

Abbreviations: HCC, hepatocellular carcinoma; AST, aspartate transaminase; ALT, alanine transaminase; γ-GTP, γ-glutamyl transpeptidase; CT, computed tomography; NAFLD, nonalcoholic fatty liver disease; SS, simple steatosis; NASH, nonalcoholic steatohepatitis; CE-TOFMS, capillary electrophoresis time-of-flight mass spectrometry; GSH, reduced glutathione; GC, gastric cancer; GCS, γ-glutamylcysteine synthetase; C, healthy control; DI, drug-induced liver injury; AHB, asymptomatic hepatitis B virus infection; CHB, chronic hepatitis B; CNALT, hepatitis C with persistently normal alanine transaminase; CHC, chronic hepatitis C; CIR, cirrhosis type C; HBs, hepatitis B surface; HBV, hepatitis B virus; HCV, hepatitis C virus; AFP, α-fetoprotein; PIVKA, protein induced by vitamin K antagonist; LC–MS/MS, liquid chromatography–electrospray tandem mass spectrometry; MLR, multiple logistic regression; APAP, acetaminophen; GS, glutathione synthetase; BSO, buthionine sulfoximine; DEM, diethylmaleate; ROS, reactive oxygen species.

Introduction

Acute or chronic viral hepatitis affects populations around the world, and the disease often progresses from chronic hepatitis and cirrhosis to hepatocellular carcinoma (HCC) [1]. Accurate diagnosis at earlier stages is necessary for improved therapeutic outcome. However, the diagnostic procedures are laborious and not risk-free. Patients with suspected liver damage are initially subjected to liver function tests that include the assessment of aspartate transaminase (AST), alanine transaminase (ALT), and γ-glutamyl transpeptidase (γ-GTP) serum levels. If these levels are abnormal, patients are then subjected to diagnostic imaging, such as ultrasound and computed tomography (CT), and assays to determine the presence of antibodies against hepatitis virus. Finally, a liver biopsy may be recommended to evaluate the severity of inflammation or fibrosis and to confirm the indications for antiviral therapy.

Recently, nonalcoholic fatty liver disease (NAFLD) has become the most common liver disease in western countries. It

encompasses a wide spectrum of conditions associated with over-accumulation of fat in the liver, ranging from simple steatosis (SS) to nonalcoholic steatohepatitis (NASH), and cirrhosis [2]. Although SS typically follows a benign non-progressive clinical course, NASH may eventually develop into cirrhosis and HCC. To date, a liver biopsy remains the gold standard for the diagnosis of NASH [3]. However, since the biopsy procedures carry the risk of mortality [4,5], the noninvasive identification of biomarkers, that can provide reliable differential diagnoses for the characterization of liver diseases, is desirable.

Metabolomics, which can be defined as measurement of the levels of all cellular metabolites, has emerged as a powerful new tool for discovering new low molecular weight biomarkers. Its utility has been demonstrated by the identification of new biomarkers for prostate cancer [6], Parkinson's disease [7], type 2 diabetes mellitus [8], acute myocardial ischemia [9], and pre-eclampsia [10].

Recently, we developed new metabolomic profiling approaches based on capillary electrophoresis mass spectrometry [11] and capillary electrophoresis–time-of-flight mass spectrometry (CE–TOFMS) [12–14]. The efficacy of CE–TOFMS was demonstrated by the discovery of ophthalmate (γ-glutamyl-2-aminobutyrylglycine) as a biomarker; in mice, reduced glutathione (GSH) depletion produced acetaminophen-induced hepatotoxicity [12,14]. In this study, to discover new noninvasive biomarkers for human liver diseases, we comprehensively analyzed the serum metabolites in a total of 248 samples from patients with nine types of liver disease or gastric cancer (GC) and from normal individuals using our metabolomic approaches, and found increased levels of γ-glutamyl dipeptides in the majority of the liver diseases. Moreover, we found that γ-glutamyl dipeptides were synthesized via the ligation of glutamate with various amino acids and amines by the γ-glutamylcysteine synthetase (GCS), an enzyme that is feedback-inhibited by GSH, and that the levels of γ-glutamyl dipeptides were indicative of the amount of GSH production. The concentrations of serum γ-glutamyl dipeptides varied with the stage and type of liver disease and can, therefore, act as new biomarkers for liver diseases. Here, we report that a highly specific set of γ-glutamyl dipeptides, alone or in combination with transaminases and methionine sulfoxide, can effectively distinguish specific liver diseases from other hepatic injuries and healthy control samples.

Materials and methods

Serum samples

A total of 248 serum samples were obtained from three institutes, Yamagata University Hospital (YUH; Yamagata, Japan), University of Tokyo Hospital (UTH; Tokyo, Japan) and Shonai Hospital (SH; Tsuruoka, Japan). The 162 YUH cases comprised 53 healthy controls (C) and patients with drug-induced liver injury (DI; $n = 10$), asymptomatic hepatitis B virus infection (AHB; $n = 9$), chronic hepatitis B (CHB; $n = 7$), hepatitis C with persistently normal alanine transaminase (CNALT; $n = 10$), chronic hepatitis C (CHC; $n = 24$), cirrhosis type C (CIR; $n = 10$), HCC ($n = 19$), SS ($n = 9$) and NASH ($n = 11$). The 75 UTH cases comprised four controls and patients with DI ($n = 17$), AHB ($n = 7$), CHB ($n = 7$), CNALT ($n = 8$), CHC ($n = 11$), CIR ($n = 8$) and HCC ($n = 13$). The 11 SH cases were all GC patients. Written informed consent was obtained from all the participants and the study protocol conformed to the ethical guidelines of the 1975 Declaration of Helsinki as reflected in a priori approval by the appropriate institutional review boards of YUH, UTH, and SH. The study subjects were patients with viral liver diseases, drug-induced hepatotoxicity or NAFLD who were referred to the Department of Gastroenterology and Hepatology at YUH, UTH, or SH.

Clinical diagnosis

All the healthy controls had normal liver function and no viral hepatitis infection, and none were alcoholics. The AHB and CNALT patients were confirmed to have normal liver function and to be positive for hepatitis B surface (HBs) antigen and hepatitis B virus (HBV) DNA, or for anti-hepatitis C virus (HCV) antibodies and HCV RNA, respectively. DI was diagnosed based on abnormal values on biochemical tests, absence of other hepatic diseases, and a history of treatment with drugs suspected of being probable causes of DI. The suspected medications were different, and the biochemical test results in each patient normalized after their withdrawal.

CHC and CIR were diagnosed on the basis of physical examination, biochemical tests, ultrasonography, and CT findings. Some patients with chronic hepatitis provided informed consent for a liver biopsy, and the procedure was performed to confirm the accuracy of the diagnosis. The diagnosis of CHB and CHC was based on increased ALT levels (above the upper limit of the normal range) in at least two blood samples assayed over a 6-month period, and the presence of detectable HBs antigen and HBV DNA or detectable anti-HCV antibodies and HCV RNA, respectively. HCV infection was causative in all cirrhosis patients, and they manifested symptoms of portal hypertension, such as splenomegaly, esophageal varices, encephalopathy, or ascites.

The diagnosis of HCC was based on ultrasonography, CT, and MRI findings that revealed features typical of HCC. HCV was causative in all cases, and the α-fetoprotein (AFP) and protein induced by vitamin K antagonist (PIVKA)-II levels were assayed in all HCC patients.

All of the SS and NASH patients underwent liver biopsy. The tissue samples were stained with hematoxylin–eosin, reticulin, and Masson trichrome; and examined by the same experienced pathologist who was blinded to the clinical data. The histological criterion for the diagnosis of NAFLD was the presence of fatty changes in hepatocytes. When hepatocytes exhibited macrovesicular steatosis, the differential diagnosis was SS or NASH. The criteria for a diagnosis of steatohepatitis were the presence of lobular inflammation and either ballooning cells or perisinusoidal/pericellular fibrosis, in addition to steatosis in the liver specimen. No patient with autoimmune hepatitis, primary biliary cirrhosis, sclerosing cholangitis, hemochromatosis, α1-antitrypsin deficiency, Wilson's disease, or alcoholic liver injury was included. All patients with GC were diagnosed by pathologic studies of biopsy tissues.

Analytical and statistical technologies for biomarker discovery

Using a total of 237 samples from YUH (training cohort, $n = 162$) and UTH (validation cohort, $n = 75$) (Table 1), we performed CE–TOFMS for a comprehensive analysis of the metabolite changes to discover new biomarkers in the diagnosis of human liver diseases. To facilitate peak identification and quantification, we analyzed 162 metabolic standards listed in the KEGG LIGAND database [15] before analyzing the samples. Global mass scanning over a 50–1000 m/z range was applied in the CE–TOFMS mode [12]. To focus on γ-glutamyl peptides, we employed a highly sensitive method using liquid chromatography electrospray tandem mass spectrometry (LC–MS/MS) with multiple reactions monitoring for analyses of the patient serum samples. The Kruskal–Wallis test and Dunn's post-test were used to assess the statistical significance of differences among C, DI, AHB, CHB, CNALT, CHC, CIR, and HCC. The Mann–Whitney test was used to evaluate the statistical significance of differences between SS and NASH. The algorithm of the feature selection for the multiple logistic regression (MLR) models is described in the Supplementary data.

Results

Discovery of γ-glutamyl dipeptides in serum by metabolomic profiling

The CE–TOFMS analysis quantified the levels of 49 metabolites in the serum samples (Supplementary Tables 1 and 2) and revealed increases in many compounds in most liver diseases. We identified these compounds as γ-glutamyl dipeptides (e.g., γ-Glu-Gly, γ-Glu-Ala, γ-Glu-Ser, γ-Glu-Val, γ-Glu-Thr, γ-Glu-Taurine, γ-Glu-Leu, γ-Glu-Gln, γ-Glu-Lys, γ-Glu-Glu, γ-Glu-Met, γ-Glu-His, γ-Glu-Phe, γ-Glu-Arg, γ-Glu-Citrulline, γ-Glu-Tyr, and γ-Glu-Trp) by comparing their migration times and exact molecular

Table 1. Summary of patient information.

Clinical information		Training cohort (n = 162)	Defect no.	Validation cohort (n = 75)	Defect no.	*p* value
Age (years)						
	Median	61	0	66	0	0.47
	Interquartile range	51-73	0	55-70	0	
Sex (n)	Male	73	0	52	0	0.0007*
	Female	89	0	23	0	
AST (UL^{-1})						
	C	21.5 ± 5.40	0	25.3 ± 3.60	0	0.074
	DI	274 ± 567	0	81.2 ± 84.9	0	0.15
	AHB	25.0 ± 6.81	2	23.9 ± 6.90	0	0.71
	CHB	109 ± 164	0	150 ± 146	0	0.0059
	CNALT	24.1 ± 3.80	0	23.8 ± 6.00	0	0.72
	CHC	62.8 ± 65.3	0	110 ± 51.0	0	0.0010
	CIR	54.6 ± 27.1	0	58.0 ± 26.1	0	0.69
	HCC	71.3 ± 52.8	0	35.0 ± 24.5	0	0.0010
	SS	41.2 ± 11.5	0			
	NASH	78.6 ± 48.0	0			
ALT (UL^{-1})						
	C	17.7 ± 4.70	0	25.0 ± 8.30	0	0.062
	DI	253 ± 343	0	115 ± 132	0	0.15
	AHB	26.6 ± 18.6	2	23.1 ± 5.60	0	0.40
	CHB	117 ± 162	0	173 ± 131	0	0.0060
	CNALT	17.9 ± 4.10	0	21.5 ± 3.60	0	0.074
	CHC	79.4 ± 81.0	0	160 ± 116	0	0.0036
	CIR	40.7 ± 21.9	0	57.3 ± 42.4	0	0.69
	HCC	57.9 ± 58.8	0	25.0 ± 21.6	0	0.0026
	SS	72.2 ± 24.5	0			
	NASH	121 ± 140	0			
γ-GTP						
	C	20.7 ± 8.60	0	—	4	—
	DI	190 ± 236	0	46.2 ± 29.5	5	0.010
	AHB	31.1 ± 24.1	2	—	7	—
	CHB	52.8 ± 38.1	1	—	7	—
	CNALT	150 ± 5.70	0	—	8	—
	CHC	48.5 ± 36.4	0	—	11	—
	CIR	28.8 ± 17.9	0	49.6 ± 53.1	0	0.17
	HCC	51.2 ± 31.1	0	—	13	—
	SS	61.8 ± 43.7	0			
	NASH	98.7 ± 99.1	0			
AFP						
	CHC	6.40 ± 7.40	3	—	11	—
	CIR	35.1 ± 71.8	0	14 ± 15.6	0	0.63
	HCC	9.79×10^2 ± 1.73×10^3	0	7.04×10^3 ± 2.52×10^4	0	0.024
PIVKA-II						
	HCC	1.57×10^2 ± 1.87×10^2	0	7.78×10^3 ± 2.77×10^4	0	0.022

*Chi-square test. The others *p* values were obtained by the Mann–Whitney *U*-test.

Fig. 1. Heat map representing the hierarchical clustering of 67 compounds in serum samples from controls and patients with various types of liver disease in both cohorts. Each row shows data for a specific metabolite or transaminase, and each column shows data for the healthy controls and patients with liver diseases. The compound concentration in each individual was divided by the average concentration in the healthy controls and the obtained values were then averaged again for each disease. The metabolites highlighted in blue showed large fold changes (disease/control ratios of >2.5) in an average of seven liver diseases. $^{*}p$ <0.05, $^{**}p$ <0.01, $^{***}p$ <0.0001, significance difference by the Kruskal–Wallis test. The compounds were clustered based on elucidation distances. Red and green denote relatively high and low concentrations, respectively, compared with the average concentration.

weights with those of the standards. Significant differences were observed among controls and liver diseases (p <0.0001; Kruskal–Wallis test) except for γ-Glu-Met in the validation data (Supplementary Tables 1 and 2). Correlational cluster analyses of 67 compounds showed that all the γ-glutamyl dipeptides except for γ-Glu-Tyr and γ-Glu-Trp were clustered with AST, ALT, and metabolites involved in oxidative stress responses, namely glucosamine [16] and methionine sulfoxide [17–19] (Fig. 1).

Statistical analysis and validation for biomarker discovery

From the serum samples obtained at YUH, we selected 89 liver disease patients including DI, AHB, CHB, CNALT, CHC, CIR, and HCC patients, and 53 healthy controls with no significant differences in the age distribution between the training and validation cohorts (Table 1). As shown in the whisker box plots for the training cohort (Fig. 2), the levels of γ-glutamyl dipeptides and of AST and ALT, as commonly used hepatocyte biomarkers, were increased in different patterns in comparison with C. For example, the AST and ALT levels were significantly increased in patients with DI, CHB, CHC, CIR, and HCC (p <0.05; Dunn's post-test), but not in those with AHB and CNALT (Fig. 2). On the other hand, significant increases were observed in the levels of γ-Glu-Ser, γ-Glu-Val, γ-Glu-Thr, γ-Glu-Leu, and γ-Glu-Phe (p <0.05; Dunn's post-test) in AHB and in the levels of all the γ-glutamyl derivatives of amino acids (p <0.05; Dunn's post-test) except for ophthalmate, γ-Glu-Thr, and γ-Glu-Trp in CNALT (Fig. 2 and Supplementary Table 1). Oxidative metabolites, methionine sulfoxide, and glucosamine were significantly increased in all diseases (p <0.05; Dunn's post-test) and in CHB, CNALT, and CHC (p <0.0001; Dunn's post-test), respectively (Fig. 2).

To assess their abilities to discriminate specific liver diseases from other liver diseases, we developed MLR models using combinations of several components of the γ-glutamyl dipeptides, transaminases, and oxidative metabolites using the training dataset. For example, an MLR model incorporating four selected biomarkers (γ-Glu-Ala, γ-Glu-Citrulline, γ-Glu-Thr, and γ-Glu-Phe) was able to differentiate HCC from the other groups (C, DI, AHB, CHB, CNALT, CHC, and CIR) with an area under the receiver-operating characteristic (ROC) curve (AUC) value of 0.762 (95% CI 0.647–0.877, p = 0.00025). The probability (p) of HCC is calculated by: $\log(p/(1-p)) = -1.87 - 1.13 \times$ γ-Glu-Ala $+ 3.51 \times$ γ-Glu-Citrulline $- 1.65 \times$ γ-Glu-Thr $+ 6.99 \times$ γ-Glu-Phe (Table 2). When the concentrations of γ-Glu-Ala, γ-Glu-Citrulline, γ-Glu-Thr, and γ-Glu-Phe are 1.7, 0.84, 0.54, and 0.34 μM, respectively, the probability of HCC is 65.5%. All the MLR models achieved high AUC values at statistically significant levels (between 0.754 and 0.972, p <0.011) (Fig. 3, Table 2 and Supplementary Table 3).

The developed MLR models were evaluated in a blinded manner using an independent cohort (YUH) consisting of 75 individuals who were not members of the training cohort (Supplementary Table 2). We found that all of the MLR models also produced high AUC values at statistically significant levels (between 0.707 and 0.993, p <0.023) (Fig. 3, Table 2 and Supplementary Table 3). Although C, CHB, and CHC were each differentiated from the other groups by a single γ-glutamyl dipeptide (γ-Glu-Phe, γ-Glu-Thr, and γ-Glu-Lys, respectively), the MLR models for the other diseases required multiple biomarkers to achieve accurate discrimination (Table 2). The odds ratios of ALT, AST, and methionine sulfoxide were close to 1.0 compared with the odds ratios of the γ-glutamyl dipeptides, indicating their

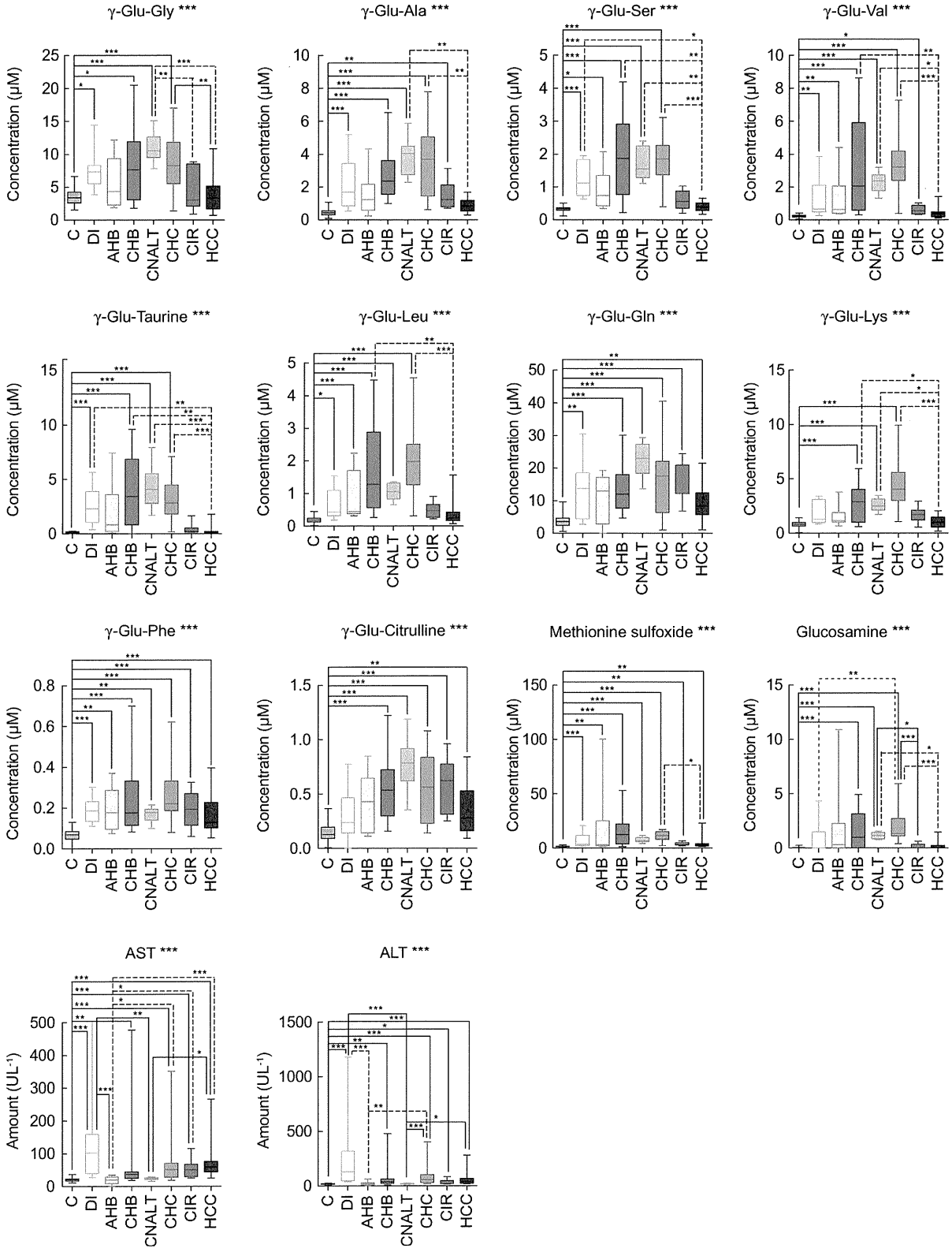
γ-Glu-Gly ***
γ-Glu-Ala ***
γ-Glu-Ser ***
γ-Glu-Val ***
γ-Glu-Taurine ***
γ-Glu-Leu ***
γ-Glu-Gln ***
γ-Glu-Lys ***
γ-Glu-Phe ***
γ-Glu-Citrulline ***
Methionine sulfoxide ***
Glucosamine ***
AST ***
ALT ***
Concentration (μM)
Amount (UL-1)
C
DI
AHB
CHB
CNALT
CHC
CIR
HCC

Table 2. Biomarkers for discriminating each liver disease selected by MLR models.

Group	Biomarker	Coefficient	95% CI		Odds ratio	95% CI		*p* value
C	(Intercept)	5.77	3.84	8.32	—	—	—	<0.0001
	γ-Glu-Phe	-58.2	-84.3	-39.0	5.16×10^{-26}	2.47×10^{-37}	1.15×10^{-17}	<0.0001
DI	(Intercept)	-3.08	-4.49	-1.94	—	—	—	<0.0001
	ALT	0.020	7.89×10^{-3}	0.034	1.02	1.01	1.03	2.00×10^{-3}
	γ-Glu-Citrulline	-1.55	-5.01	1.13	0.21	6.68×10^{-3}	3.11	0.31
AHB	(Intercept)	-1.52	-3.35	0.63	—	—	—	0.12
	AST	-0.057	-0.15	-4.96×10^{-3}	0.94	0.86	1.00	0.12
	Methionine sulfoxide	0.072	0.018	0.15	1.08	1.02	1.17	0.047
CHB	(Intercept)	-4.52	-6.33	-3.24	—	—	—	<0.0001
	γ-Glu-Thr	1.52	0.65	2.63	4.58	1.91	13.9	2.30×10^{-3}
CNALT	(Intercept)	-0.76	-3.15	1.94	—	—	—	0.55
	ALT	-0.16	-0.34	-0.049	0.85	0.71	0.95	0.032
	γ-Glu-Taurine	0.80	0.43	1.31	2.23	1.54	3.72	3.00×10^{-4}
CHC	(Intercept)	-4.73	-6.39	-3.47	—	—	—	<0.0001
	γ-Glu-Lys	1.27	0.85	1.82	3.57	2.34	6.14	<0.0001
CIR	(Intercept)	-2.79	-4.05	-1.55	—	—	—	<0.0001
	γ-Glu-Ala	1.80	0.42	3.52	6.05	1.52	33.7	0.020
	γ-Glu-Leu	-0.066	-3.06	2.24	0.94	0.047	9.42	0.96
	γ-Glu-Ser	-1.35	-5.35	1.86	0.26	4.77×10^{-3}	6.44	0.41
	γ-Glu-Taurine	-2.28	-5.07	-0.33	0.10	6.27×10^{-3}	0.72	0.064
HCC	(Intercept)	-1.87	-2.90	-0.90	—	—	—	2.00×10^{-4}
	γ-Glu-Ala	-1.13	-2.44	-0.14	0.32	0.087	0.87	0.050
	γ-Glu-Citrulline	3.51	0.45	7.00	33.4	1.57	1.10×10^{3}	0.033
	γ-Glu-Thr	-1.65	-5.12	0.49	0.19	5.95×10^{-3}	1.63	0.27
	γ-Glu-Phe	6.99	-0.52	14.7	1.09×10^{3}	5.92×10^{-1}	2.50×10^{6}	0.063

Note: The en-dashes in the 95% CI columns indicate that these values could not be calculated. Biomarker and coefficients are used in MLR model to calculate the probability of each disease. Intercept indicates the constant term in MLR models.

relatively lower contributions to the separation ability of the MLR models (Table 2). Overall, for all types of liver diseases, the MLR models mostly based on γ-glutamyl dipeptides provided complementary results, even in the second (validation) cohort.

γ-Glutamyl dipeptides as biomarkers for HCC and NAFLD

To evaluate the diagnostic potential of γ-glutamyl dipeptides for HCC, we compared their diagnostic abilities with that of AFP, an established marker for HCC (Fig. 4). We found that the MLR models using four γ-glutamyl dipeptides (γ-Glu-Ala, γ-Glu-Citrulline, γ-Glu-Thr, γ-Glu-Phe) (Table 2) were better at distinguishing HCC from CHC and CIR (AUC = 0.881) than AFP (AUC = 0.760) (Fig. 4).

We further investigated the biomarker specificities by comparing the serum γ-glutamyl dipeptide levels in GC and HCC patients (Supplementary Fig. 2 and Table 4). The analyses revealed significant differences, with the exception of γ-Glu-Phe, and the levels of γ-glutamyl dipeptides were notably low in GC.

Differences in the levels of γ-glutamyl dipeptides were also observed in NAFLD. The levels of six γ-glutamyl dipeptides (γ-Glu-Val, γ-Glu-Thr, γ-Glu-Leu, γ-Glu-His, γ-Glu-Phe, and γ-Glu-Arg) were significantly higher (p <0.05; Mann–Whitney test) in SS than in NASH (Supplementary Fig. 3 and Table 5). Although further investigations are necessary, these dipeptides can be used as noninvasive biomarkers in rapid screening for SS and NASH.

Mechanism of γ-glutamyl dipeptide biosynthesis

To confirm the γ-glutamyl dipeptide biosynthesis pathway, the hepatic metabolism was investigated using a mouse model. In

Fig. 2. Representative whisker box plots of the serum levels of detected transaminases and metabolites in the training cohort. The horizontal lines indicate the upper median, median, and lower median, and the whiskers show the maximum and minimum levels. One plot for AST was outside the range (>500 U/L). *p <0.05, **p <0.01, ***p <0.0001, significance difference by the Kruskal–Wallis test and Dunn's post-test for each marker and two groups in each marker, respectively.

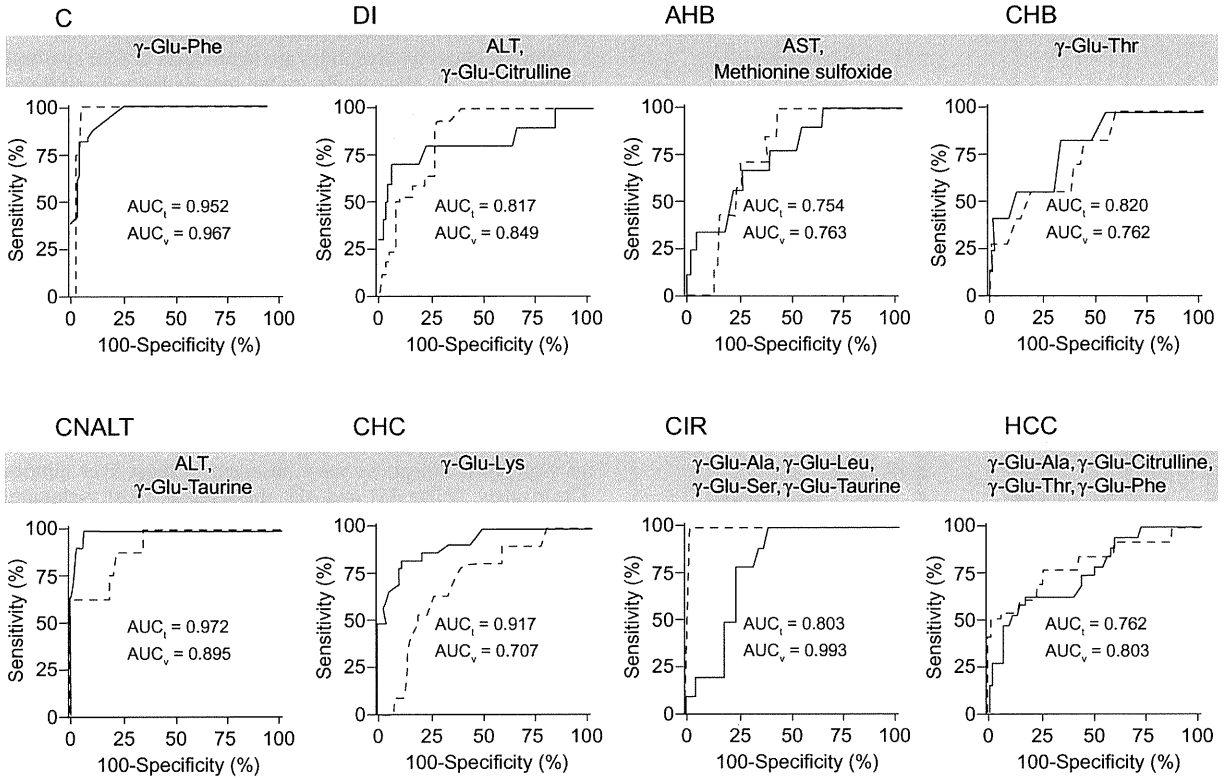

Fig. 3. ROC curve analyses of the ability of γ-glutamyl peptides alone or in combination with AST, ALT and methionine sulfoxide to discriminate each group from all other liver diseases and healthy controls. The solid and dashed curves represent the ROC curves for the training and validation cohorts, respectively. AUCt and AUCv in each panel indicate the AUC values in the training and validation cohorts, respectively. The group label indicates the discriminated group from all the other groups by an MLR model. The biomarkers in each panel were used in the MLR model for discriminating the group, e.g., ALT and γ-Glu-Taurine were the biomarkers for discriminating CNALT from the other groups. The coefficients and constant term of the MLR model of these biomarkers were summarized in Table 2.

acetaminophen (APAP)-treated mice [12], ophthalmate, a γ-glutamyl tripeptide, was synthesized through consecutive reactions with GCS and glutathione synthetase (GS), the same enzymes that play a role in GSH synthesis [12] (Fig. 5). Therefore, we investigated the alterations in the levels of hepatic amino acids, amines, γ-glutamyl dipeptides, and tripeptides after administration of buthionine sulfoximine (BSO), diethylmaleate (DEM) or APAP (Supplementary Fig. 4). BSO treatment resulted in GCS inhibition [20] and marked reductions in most of the hepatic γ-glutamyl dipeptide and tripeptide levels (Fig. 5 and Supplementary Fig. 4A). In contrast, DEM treatment led to GSH depletion by oxidation of the thiol group in GSH [21], resulting in GCS activation and considerable increases in the hepatic γ-glutamyl dipeptide and tripeptide levels compared with the controls (Fig. 5 and Supplementary Fig. 4A). The hepatic levels of several γ-glutamyl dipeptides and tripeptides were increased with concurrent GSH depletion in APAP-treated mice (Supplementary Fig. 4B and C). These results indicated that in mice, γ-glutamyl dipeptides and tripeptides were certainly synthesized via the ligation of glutamate by various amino acids through consecutive reactions with GCS and GS when GSH was depleted (Fig. 5). The identification details for the γ-glutamyl dipeptide biosynthetic pathway are described in the Supplementary data.

Discussion

Our analyses of 237 serum samples from patients with liver diseases and healthy controls revealed that γ-glutamyl dipeptides were increased in liver injuries and could provide specific information for different liver diseases. In APAP-induced liver injury in mice, ophthalmate, a γ-glutamyl tripeptide, was markedly increased as a byproduct of GSH synthesis [21] (Fig. 5 and Supplementary Fig. 4B). However, in liver diseases in humans, many γ-glutamyl dipeptides were primarily synthesized and secreted from hepatocytes into the blood (Figs. 1 and 5). Although the reason for the difference is unclear, it may be attributable to species differences in the levels and activities of enzymes and transporters [22,23].

In all types of liver disease, oxidative stress resulting from an imbalance between the production of reactive oxygen species (ROS) and the ability of a biological system to detoxify reactive intermediates plays a crucial role in the induction and progression of liver damage independently of its etiology [1]. In patients with hepatitis, oxidative stress is produced by inflammation induced by immunological mechanisms. Upon viral infection, NADPH oxidase produces ROS in neutrophils and macrophages, and ROS are also generated from free iron through the Fenton reaction [24–26]. ROS are further produced in hepatocytes upon

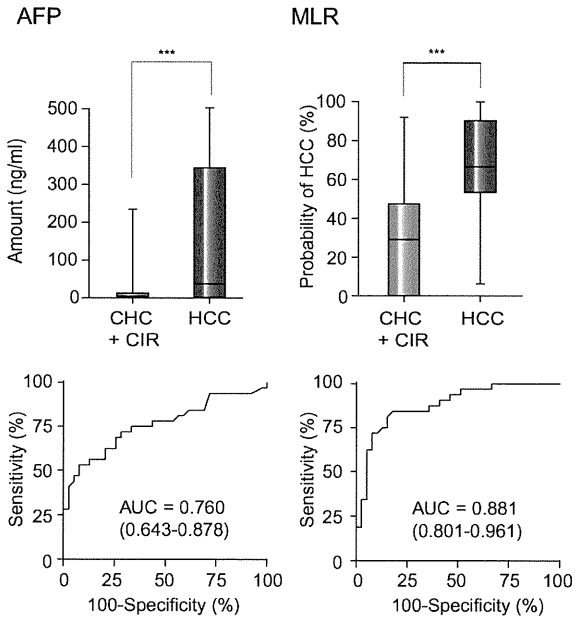

Fig. 4. Whisker box plots and ROC curves of AFP and MLR analyses based on γ-Glu-Ala, γ-Glu-Citrulline, γ-Glu-Thr and γ-Glu-Phe for discriminating patients with HCC (n = 32) from patients with CHC (n = 35) and CIR (n = 18).

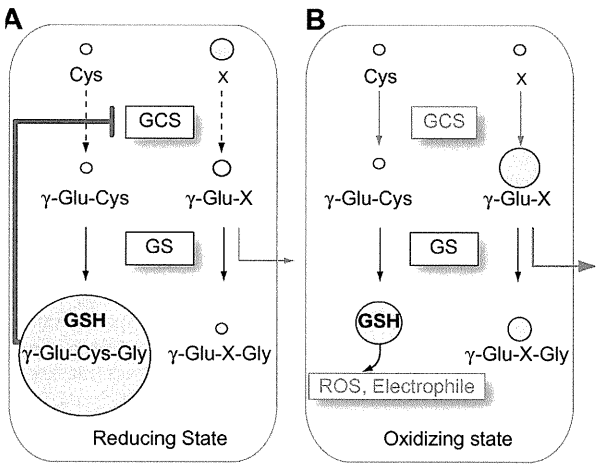

Fig. 5. Biosynthetic mechanism of γ-glutamyl peptides in hepatocytes under (A) reducing conditions and (B) oxidative stress. GCS is feedback-inhibited by GSH under reducing conditions and small amounts of γ-glutamyl dipeptides are synthesized. During oxidative stress, GSH is consumed, leading to GCS activation. This could result in biosynthesis of γ-glutamyl dipeptides, which are then effluxed across the hepatocellular membrane. γ-Glutamyl dipeptides and tripeptides are indicated by γ-Glu-X and Glu-X-Gly, respectively (X = amino acid or amine).

the release of inflammatory cytokines, such as tumor necrosis factor-α and interleukin-1β from inflammatory cells [27]. GSH is the most abundant antioxidant in hepatocytes, and helps to protect cells against ROS. Upon depletion of GSH, ROS induce oxidative stress resulting in liver damage, and reduced GSH levels have been demonstrated in various liver diseases [28–30].

Since γ-glutamyl dipeptides are byproducts of GSH synthesis catalyzed by GCS, their levels are indirect evidence for GSH production (Fig. 5). Different levels of γ-glutamyl dipeptides were observed in different types of liver disease and each γ-glutamyl dipeptide showed a somewhat different variation pattern among liver diseases (Fig. 2). This might be attributed to differences in hepatic levels of amino acids (the substrate of GCS) among liver diseases, though further studies are necessary to understand the details of this observation.

In healthy controls, the γ-glutamyl dipeptide levels were low. This occurred because under reducing conditions, the level of hepatic GSH was high and a small amount of GSH was biosynthesized (Fig. 5A). However, in the patients with liver diseases, GSH was consumed to neutralize the generated ROS, which in turn led to GCS activation, resulting in the biosynthesis of GSH together with γ-glutamyl dipeptides (Fig. 5B). Therefore, increased levels of γ-glutamyl dipeptides were observed in most liver injuries. Surprisingly, unlike AST and ALT, the levels of most γ-glutamyl dipeptides were markedly increased in asymptomatic individuals with AHB and CNALT (Fig. 2 and Supplementary Fig. 1), possibly because viral infection induced ROS generation followed by GSH depletion, which led to the biosynthesis of GSH and γ-glutamyl dipeptides (Fig. 5). We hypothesize that sufficiently high levels of GSH production neutralized ROS, resulting in lower incidences of AHB and CNALT.

There are relationships between liver diseases attributable to HCV infection and oxidative stress parameters, such as ROS, antioxidants, and inflammation. Oxidative stress increased with hepatic disease progression in HCV-infected patients [31]. Consistent with that report, among all the patients with HCV-related liver diseases, the serum levels of γ-glutamyl dipeptides, as indicators of hepatic GSH production, were markedly increased in CNALT and tended to decrease with disease progression (CNALT ⩾ CHC > CIR > HCC) (Fig. 2). These observations led us to conclude that at the time of viral infection (CNALT), a sufficient amount of GSH production can neutralize ROS and thus weaken the pathogenesis of liver damage. However, when GSH production falls below ROS generation, oxidative stress followed by inflammation is induced, resulting in the development and progression of liver diseases. Similarly, the levels of several γ-glutamyl dipeptides were significantly lower in NASH patients than in SS patients (Supplementary Fig. 3), indicating low levels of GSH production in NASH patients. Based on the present observations, we suggest that NASH is susceptible to oxidative stress and progression to liver fibrosis and cirrhosis.

HCC is one of the most common cancers in humans, and primarily develops in patients with chronic liver disease. Its early detection is important because effective treatments are available for the management of non-advanced cancers [32]. Until now, the diagnosis of HCC has relied on combinations of imaging techniques and measurements of the serum levels of AFP [33] and PIVKA-II [34]. Although they are reliable tumor markers for the diagnosis and monitoring of primary HCC, high levels of serum AFP and plasma PIVKA-II have also been observed in some gastric carcinomas [34,35]. However, the serum γ-glutamyl dipeptide levels in GC and HCC patients revealed significant differences, and the levels of several γ-glutamyl dipeptides was notably low in GC (Supplementary Fig. 2). We suspect that this occurred through differences in the tissue activities of the glutathione

system, since GSH is mainly synthesized *de novo* in the liver, and hypothesize that the γ-glutamyl dipeptide levels may reflect hepatic dysfunction.

Drug-induced hepatotoxicity is a frequent cause of liver injury, and the predominant clinical presentation is acute hepatitis and/or cholestasis. Overdoses of APAP, the most commonly used analgesic and antipyretic, can lead to possibly fatal hepatitis and several hundred deaths attributable to this drug occur annually in the United States. Our DI samples were from patients with so-called idiosyncratic hepatotoxicity, and the underlying mechanisms of this disease remain unclear. Interestingly, the changes in the serum levels of γ-glutamyl dipeptides were similar among the DI samples although the causative drugs differed widely and the mechanisms responsible for the development of hepatotoxicity may also be different. Our findings revealed that the amount of γ-glutamyl dipeptide production attributable to a reduction in the hepatocellular GSH concentration was a common feature in drug-induced idiosyncratic hepatotoxicity. With AUC values of 0.817 (training data) and 0.849 (validation data) (Supplementary Table 3), the serum levels of ALT and γ-Glu-Citrulline could be used to distinguish between DI patients on the one hand and patients with viral hepatitis infection and healthy controls on the other (Table 2). Therefore, we suggest that these compounds represent noninvasive biomarkers that facilitate rapid screening for DI.

In summary, our CE–TOFMS and LC–MS/MS metabolomics-based analyses of serum samples from patients with liver diseases showed quantitative differences in γ-glutamyl dipeptides in various liver diseases. Our highly specific set of γ-glutamyl dipeptides, transaminases, and methionine sulfoxide enabled us to discriminate among liver diseases including DI, AHB, CHB, CNALT, CHC, CIR, and HCC, indicating that they can be used as multiple biomarkers in rapid screening for different types and stages of liver disease. Furthermore, we have shown that γ-glutamyl dipeptide synthesis was catalyzed by GCS, the enzyme that is feedback-inhibited by GSH, and thus the levels of these biomarkers were indicative of hepatic GSH production. As observed in patients with HCV-related liver diseases and NAFLD, the serum γ-glutamyl dipeptide levels tended to decrease during the course of liver disease progression, indicating an increase in oxidative stress resulting from decreased GSH production during liver disease progression. Therefore, γ-glutamyl dipeptide measurement can potentially provide valuable information about the hepatic reduction–oxidation state to gain insights into the role of oxidative stress in the pathogenesis and progression of liver diseases.

Conflict of interest

The Authors who have taken part in this study declared that they do not have anything to disclose regarding funding or conflict of interest with respect to this manuscript.

Financial support

This work was supported by Health and Labour Sciences Research Grants "Research on Biological Markers for New Drug Development" (T.S.) and "Research on Risk of Chemical Substances" (T.S.). Additional support was obtained through grants from the Ministry of Education, Culture, Sports, Science and Technology (MEXT) for a Global COE Program entitled "Human Metabolomic Systems Biology" in Life Sciences (T.S., M.T. and M.S.) and the ERATO Gas Biology Project (M.S.), as well as research funds from the Yamagata Prefectural Government and City of Tsuruoka.

Supplementary data

Supplementary data associated with this article can be found, in the online version, at doi:10.1016/j.jhep.2011.01.031.

References

[1] Loguercio C, Federico A. Oxidative stress in viral and alcoholic hepatitis. Free Radic Biol Med 2003;34:1–10.
[2] Brunt EM. Nonalcoholic steatohepatitis. Semin Liver Dis 2004;24:3–20.
[3] Younossi ZM, Jarrar M, Nugent C, Randhawa M, Afendy M, Stepanova M, et al. A novel diagnostic biomarker panel for obesity-related nonalcoholic steatohepatitis (NASH). Obes Surg 2008;18:1430–1437.
[4] Piccinino F, Sagnelli E, Pasquale G, Giusti G. Complications following percutaneous liver biopsy. A multicentre retrospective study on 68,276 biopsies. J Hepatol 1986;2:165–173.
[5] Bolukbas C, Bolukbas FF, Horoz M, Aslan M, Celik H, Erel O. Increased oxidative stress associated with the severity of the liver disease in various forms of hepatitis B virus infection. BMC Infect Dis 2005;5:95.
[6] Sreekumar A, Poisson LM, Rajendiran TM, Khan AP, Cao Q, Yu J, et al. Metabolomic profiles delineate potential role for sarcosine in prostate cancer progression. Nature 2009;457:910–914.
[7] Bogdanov M, Matson WR, Wang L, Matson T, Saunders-Pullman R, Bressman SS, et al. Metabolomic profiling to develop blood biomarkers for Parkinson's disease. Brain 2008;131:389–396.
[8] Wang C, Kong H, Guan Y, Yang J, Gu J, Yang S, et al. Plasma phospholipid metabolic profiling and biomarkers of type 2 diabetes mellitus based on high-performance liquid chromatography/electrospray mass spectrometry and multivariate statistical analysis. Anal Chem 2005;77:4108–4116.
[9] Sabatine MS, Liu E, Morrow DA, Heller E, McCarroll R, Wiegand R, et al. Metabolomic identification of novel biomarkers of myocardial ischemia. Circulation 2005;112:3868–3875.
[10] Kenny LC, Dunn WB, Ellis DI, Myers J, Baker PN, Consortium TG, et al. Novel biomarkers for pre-eclampsia detected using metabolomics and machine learning. Metabolomics 2005;1:227–234.
[11] Soga T, Ohashi Y, Ueno Y, Naraoka H, Tomita M, Nishioka T. Quantitative metabolome analysis using capillary electrophoresis mass spectrometry. J Proteome Res 2003;2:488–494.
[12] Soga T, Baran R, Suematsu M, Ueno Y, Ikeda S, Sakurakawa T, et al. Differential metabolomics reveals ophthalmic acid as an oxidative stress biomarker indicating hepatic glutathione consumption. J Biol Chem 2006;281:16768–16776.
[13] Soga T, Igarashi K, Ito C, Mizobuchi K, Zimmermann HP, Tomita M. Metabolomic profiling of anionic metabolites by capillary electrophoresis mass spectrometry. Anal Chem 2009;81:6165–6174.
[14] Shintani T, Iwabuchi T, Soga T, Kato Y, Yamamoto T, Takano N, et al. Cystathionine beta-synthase as a carbon monoxide-sensitive regulator of bile excretion. Hepatology 2009;49:141–150.
[15] Goto S, Okuno Y, Hattori M, Nishioka T, Kanehisa M. LIGAND: database of chemical compounds and reactions in biological pathways. Nucleic Acids Res 2002;30:402–404.
[16] Kaneto H, Xu G, Song KH, Suzuma K, Bonner-Weir S, Sharma A, et al. Activation of the hexosamine pathway leads to deterioration of pancreatic beta-cell function through the induction of oxidative stress. J Biol Chem 2001;276:31099–31104.
[17] Levine RL, Berlett BS, Moskovitz J, Mosoni L, Stadtman ER. Methionine residues may protect proteins from critical oxidative damage. Mech Ageing Dev 1999;107:323–332.
[18] Babior BM. Phagocytes and oxidative stress. Am J Med 2000;109:33–44.
[19] Vogt W. Oxidation of methionyl residues in proteins: tools, targets, and reversal. Free Radic Biol Med 1995;18:93–105.
[20] Griffith OW, Meister A. Potent and specific inhibition of glutathione synthesis by buthionine sulfoximine (*S-n*-butyl homocysteine sulfoximine). J Biol Chem 1979;254:7558–7560.
[21] Zalups RK, Lash LH. Depletion of glutathione in the kidney and the renal disposition of administered inorganic mercury. Drug Metab Dispos 1997;25:516–523.

[22] Ishizuka H, Konno K, Shiina T, Naganuma H, Nishimura K, Ito K, et al. Species differences in the transport activity for organic anions across the bile canalicular membrane. J Pharmacol Exp Ther 1999;290:1324–1330.
[23] Mainwaring GW, Williams SM, Foster JR, Tugwood J, Green T. The distribution of theta-class glutathione *S*-transferases in the liver and lung of mouse, rat and human. Biochem J 1996;318:297–303.
[24] Marrogi AJ, Khan MA, van Gijssel HE, Welsh JA, Rahim H, Demetris AJ, et al. Oxidative stress and p53 mutations in the carcinogenesis of iron overload-associated hepatocellular carcinoma. J Natl Cancer Inst 2001;93:1652–1655.
[25] Toyokuni S, Okamoto K, Yodoi J, Hiai H. Persistent oxidative stress in cancer. FEBS Lett 1995;358:1–3.
[26] Sutton A, Nahon P, Pessayre D, Rufat P, Poire A, Ziol M, et al. Genetic polymorphisms in antioxidant enzymes modulate hepatic iron accumulation and hepatocellular carcinoma development in patients with alcohol-induced cirrhosis. Cancer Res 2006;66:2844–2852.
[27] Koike K, Miyoshi H. Oxidative stress and hepatitis C viral infection. Hepatol Res 2006;34:65–73.
[28] Boya P, de la Pena A, Beloqui O, Larrea E, Conchillo M, Castelruiz Y, et al. Antioxidant status and glutathione metabolism in peripheral blood mononuclear cells from patients with chronic hepatitis C. J Hepatol 1999;31:808–814.
[29] Tanyalcin T, Taskiran D, Topalak O, Batur Y, Kutay F. The effects of chronic hepatitis C and B virus infections on liver reduced and oxidized glutathione concentrations. Hepatol Res 2000;18:104–109.
[30] Moriya K, Nakagawa K, Santa T, Shintani Y, Fujie H, Miyoshi H, et al. Oxidative stress in the absence of inflammation in a mouse model for hepatitis C virus-associated hepatocarcinogenesis. Cancer Res 2001;61:4365–4370.
[31] Sumida Y, Nakashima T, Yoh T, Nakajima Y, Ishikawa H, Mitsuyoshi H, et al. Serum thioredoxin levels as an indicator of oxidative stress in patients with hepatitis C virus infection. J Hepatol 2000;33:616–622.
[32] Bruix J. Treatment of hepatocellular carcinoma. Hepatology 1997;25:259–262.
[33] Szklaruk J, Silverman PM, Charnsangavej C. Imaging in the diagnosis, staging, treatment, and surveillance of hepatocellular carcinoma. Am J Roentgenol 2003;180:441–454.
[34] Kudo M, Takamine Y, Nakamura K, Shirane H, Uchida H, Kasakura S, et al. Des-gamma-carboxy prothrombin (PIVKA-II) and alpha-fetoprotein-producing IIc-type early gastric cancer. Am J Gastroenterol 1992;87:1859–1862.
[35] Takano S, Honda I, Watanabe S, Soda H, Nagata M, Hoshino I, et al. PIVKA-II-producing advanced gastric cancer. Int J Clin Oncol 2004;9:330–333.

Journal of Biotechnology 154 (2011) 298–303

Contents lists available at ScienceDirect

Journal of Biotechnology

journal homepage: www.elsevier.com/locate/jbiotec

Short communication

Intracellular reactivation of transcription factors fused with protein transduction domain

Masamitsu Konno[a], Shinji Masui[b,c], Tatsuo S. Hamazaki[a], Hitoshi Okochi[a,*]

[a] Department of Regenerative Medicine, Research Institute, National Center for Global Health and Medicine, 1-21-1 Toyama, Shinjuku-ku, Tokyo 162-8655, Japan
[b] Section of Molecular Biology and Cell Engineering, Department of Regenerative Medicine, Research Institute, National Center for Global Health and Medicine, Tokyo 162-8655, Japan
[c] PRESTO, Japan Science and Technology Agency, Saitama 332-0012, Japan

ARTICLE INFO

Article history:
Received 10 May 2011
Accepted 13 May 2011
Available online 23 May 2011

Keywords:
PTD
iPS cells
ES cells
Oct3/4
Sox2
TEV protease

ABSTRACT

Induction of a desired cell type by defined transcription factors (TFs) using iPS technology can be used for cell replacement therapy. However, to overcome problems such as tumor formation, genomic insertional mutagenesis by viral transduction in the induction process needs to be avoided using alternative approaches. One approach could be the direct delivery of TF protein by a protein transduction system, whereby a protein transduction domain (PTD) is fused to facilitate the penetration of cell membrane. However, fusion proteins, including TFs, are reported to be biologically less active through the interference of PTD with proper protein folding. Here, we report a proof-of-concept study in which TF proteins fused with PTDs could be reactivated by removal of PTDs from cells. We demonstrated that Sox2 and Oct3/4 proteins fused with PTD were less active in mouse embryonic stem cells. Removal of PTD by a site-specific protease, derived from tobacco etch virus (TEV), substantially restored the functionality of these proteins, proved by enhanced rescue ability for differentiation induced by endogenous *Sox2* and *Oct3/4* repression. These results suggest that, by removing a PTD inside the cells, directly delivered TF proteins may exert substantially enhanced function than presently considered.

1. Introduction

Transcription factors (TFs) regulate gene expression, and some play pivotal roles in the determination of a cellular differentiation status. In a pioneer study, Davis et al. (1987) showed that the basic helix–loop–helix (bHLH) transcription factor MyoD induced muscle-specific properties in fibroblasts. Recent examples include induction of pancreatic β-cells from adult pancreatic exocrine cells by Ngn3, Pdx1, and Mafa (Zhou et al., 2008), neural cells from fibroblasts by Ascl1, Brn2, and Myt1l (Vierbuchen et al., 2010), macrophages from fibroblasts by PU.1 and Cebpa (Feng et al., 2008), and myocardial cells from fibroblasts by Gata4, Mef2c, and Tbx5 (Ieda et al., 2010). In addition to lineage switching between differentiated cell types, introduction of TFs can induce dedifferentiation by four TFs including Oct3/4 and Sox2 (Takahashi and Yamanaka, 2006). Retrovirus or lentivirus is employed for introduction of these TFs; however integration into the host genome can lead to insertional mutagenesis and unpredictable gene activation (Okita et al., 2007). Thus, at present, these methods are unsuitable for clinical trials or pathological analysis (Hanna et al., 2007; Wernig et al., 2008).

As an alternative to viral transduction, a protein transduction system for direct delivery of TFs into target cells has been developed. To facilitate the penetration of cell membrane, fusion with a high proportion of basic amino acids, termed a protein transduction domain (PTD), is required. PTDs, reported to date include TAT derived from HIV virus (Frankel and Pabo, 1988), Antennapedia transcription factor from *Drosophila* (Derossi et al., 1996), VP22 structural protein of Herpes-simplex virus 1 (Phelan et al., 1998), and poly-arginine (Matsushita et al., 2001; Wender et al., 2000). Although protein-fused PTD such as 11R (arginine)-P53 or VP22-P53 could penetrate cells (Phelan et al., 1998; Takenobu et al., 2002), it was also pointed out that these fusion proteins were biologically less active because of the improper folding of the protein caused by PTD (Ye et al., 2002). The efficiency of establishing iPS cells by Oct3/4, Sox2, Klf4, and c-Myc protein-fused 8R (arginine) was quite low (Kim et al., 2009). Therefore, we hypothesized that PTD should be removed from cells, especially PTD fused with TF.

In this study, we employed a site-specific protease, derived from tobacco etch virus (TEV), to dissociate PTD from fusion protein in the cell. Because of the stringent sequence specificity, TEV protease has been employed in cleaving genetically engineered fusion proteins in vitro (Dougherty et al., 1988). We demonstrated that TEV

* Corresponding author. Tel.: +81 3 3202 7181x2825; fax: +81 3 3202 7192.
E-mail address: hokochi@ri.ncgm.go.jp (H. Okochi).

0168-1656/$ – see front matter © 2011 Elsevier B.V. All rights reserved.
doi:10.1016/j.jbiotec.2011.05.006

protease introduced into mouse embryonic stem (ES) cells were effective in restoring the function of TF proteins by removal of PTD, suggesting that directly delivered TF proteins may generally exert substantially enhanced functionality than presently considered.

2. Materials and methods

2.1. Cell culture

Mouse ES cells, 2TS22C, ZHBTc4, and Plat-E cells, were cultured according to the methods described by Masui et al. (2007), Niwa et al. (2000), and Morita et al. (2000), respectively.

2.2. Plasmid construction

An eleven arginine (11R) codon sequence was combined with cDNA of *Sox2* or *Oct3/4* to obtain 11RSox2 or 11ROct3/4 (Fig. 1A). Each construct was cloned into pPy vector with CAG-IB or CAG-IP to obtain pPyCAG-IB/11RSox2 or pPyCAG-IP/11ROct3/4. The TEV protease recognition sequence was inserted between the 11R sequence and *Sox2* or *Oct3/4* to obtain pPyCAG-IB/11RTEVRSox2 or pPyCAG-IP/11RTEVROct3/4 (Fig. 1C). The residual sequence after cleavage by TEV protease was ligated with the *Sox2* or *Oct3/4* sequence to obtain pPyCAG-IB/ΔTEVRSox2 or pPyCAG-IP/ΔTEVROct3/4 (Fig. 1B). These plasmids were generated through the following steps. For pPyCAG-IB/11RSox2, the 11R-Sox2 cDNA was amplified from pBRCAGIH/Sox2 using PCR with the primers 5′-11RSox2 (5′-ATACTCGAGCCACCATGGACGCAGGCGAAGGCGACGGGAGAATCTG-TACTATGGGTGATATCCAATGTATAACATGAT-3′ [XhoI site is underlined]) and 3′-Sox2 (5′-ACAGCGGCCGCTCACATGTGCGACAGGGG-CA-3′ [NotI site is underlined]). For pPyCAG-IB/ΔTEVRSox2, the ΔTEVRSox2 cDNA was amplified from pBRCAGIH/Sox2 using PCR with the primers 5′cutSox2 (5′-ATACTCGAGCCACCATGGGTGA-TATCCAATGTATAACATGAT-3′ [XhoI site is underlined]) and 3′-Sox2. For pPyCAG-IB/11RTEVRSox2, the 11RTEVRSox2 cDNA was amplified from pBRCAGIH/Sox2 using PCR with the primers 5′-11RTEVRSox2 (5′-ATACTCGAGCCACCATGGACGCAGGCGAAGG-CGACGGGAGAATCTGTACTTCCAGGGTGAGAATCTGTACTTCCAGG-GTGAGAATCTGTACTTCCAGGGTGAGAATCTGTACTATGGGTGATAT-CCAATGTATAACATGAT-3′ [XhoI site is underlined]) and 3′-Sox2. For pPyCAG-IP/11ROct3/4, the 11ROct3/4 cDNA was amplified from pBRCAGIH/Oct3/4 using PCR with the primers 5′-11ROct3/4 (5′-ATACTCGAGCCACCATGGACGCAGGCGAAGGCGACGGGAGAATCTG-TACTATGCCCACGTTCGACCAGGC-3′ [XhoI site is underlined]) and 3′-Oct3/4 (5′-ACAGCGGCCGCTCAGACATCAGAAGTAGAAA-3′ [NotI site is underlined]). For pPyCAG-IP/11RTEVROct3/4, the 11RTEVROct3/4 cDNA was amplified from pBRCAGIH/Oct3/4 using PCR with the primers 5′-11RTEVROct3/4 (5′-ATACTCGAGCC-ACCATGGACGCAGGCGAAGGCGACGGGAGAATCTGTACTTCCAGGG-TGAGAATCTGTACTTCCAGGGTGAGAATCTGTACTTCCAGGGTGAGA-ATCTGTACTATGCCCACGTTCGACCAGGC-3′ [XhoI site is underlined]) and 3′-Oct3/4. For pPyCAG-IP/ΔTEVROct3/4, the ΔTEVROct3/4 cDNA was amplified from pBRCAGIH/Oct3/4 using PCR with the primers 5′-ΔTEVROct3/4 (5′-ATACTCGAG-CCACCATGCCCACGTTCGACCAGGC-3′ [XhoI site is underlined]) and 3′-Oct3/4. These cloning products were digested with XhoI and NotI.

Three different mutations in TEV protease cDNA were combined with drug resistance genes for hygromycin or histidinol. Six plasmid constructs, pMYsIH/TEV protease S219D mutant, pMYsIH/TEV protease S219P mutant, pMYsIH/TEV protease S219V mutant, pMYsIHisD/TEV protease S219D, pMYsIHisD/TEV protease S219P, and pMYsIHisD/TEV protease S219V mutant were generated through the following steps. For pMYsIH/TEV protease S219D and pMYsIHisD/TEV protease S219D, the TEV protease S219D cDNA was amplified from pRK603 (Addgene) using PCR with the primers 5′-S219D (5′-TTTGTCGACATGGGAGAAAGCTTGTTTAA-3′ [SalI site is underlined]) and 3′-S219D (5′-TTTGCGGCCGCATTAATTCATGAGTTGAGTC-3′ [NotI site is underlined]). For pMYsIH-IH/TEV protease S219P or S219V and pMYsIHisD/TEV protease S219P or S219V, the TEV protease S219P or S219V cDNA was amplified from pRK792 (Addgene) or pRK793 (Addgene) using PCR with the primers 5′-S219P (5′-TTTGTCGACGGTCATCATCATCATCATCA-3′ [SalI site is underlined]) and 3′-S219D (5′-TTTGCGGCCGCTTAGCGACGGCGACGACGAT-3′ [NotI site is underlined]).

2.3. Retroviral infection

Retroviral supernatant were prepared from Plat-E cells as described by Takahashi and Yamanaka (2006). Two days after infection, we initiated selection of 2TS22C using 0.1 mg/ml hygromycin (Invivogen) or ZHBTc4 using 3 mM histidinol (Sigma). The selection of clones was performed over a period of 2 weeks.

2.4. RT-PCR

The expression of TEV protease gene and the pluripotency marker genes *Oct3/4* and *Nanog* was determined by RT-PCR. Total RNA was extracted using Isogen (Nippon Gene) as described by the manufacturer and then treated with High-Capacity RNA-to-cDNA kit (AB gene) to generate cDNA. Then PCR amplification was performed for the three types of TEV protease mutant gene. PCR cycles were as follows: 95 °C for 5 min, 95 °C for 30 s, annealing temperature for 30 s, 72 °C for 1 min (25–30 cycles), and 72 °C for 3 min. The RT-PCR products were analyzed using 1% agarose gel electrophoresis and visualized with ethidium bromide. Primers used in this study are *TEVprotease* (S219V and S219P) (5′-CACTCAGCATCGAATTTCACCAA-3′ and 5′-GCTGAAAAGGCTCTTCAGGTTTC-3′), *TEVprotease* (S219D) (5′-TACA-CTCAGCATCGAATTTCACCAA-3′ and 5′-AAAAGGCTCTTCAGGTTT-GTCCA-3′), *GAPDH* (5′-TGAAGGTCGGTGTGAACGGATTTGGC-3′ and 5′-CATGTAGGCCATGAGGTCCACCA-3′), and *Nanog* (5′-GTAGC-TGTCTTCAGACACTCC-3′ and 5′-AATTAGAGCTATGCAGAGAAA-3′).

2.5. TF rescue experiment

Sox2 and *Oct3/4* repression was induced by the addition of tetracycline (Tc) (1 μg/ml) to 2TS22C and ZHBTc4 culture media (Masui et al., 2007; Niwa et al., 2000). Plasmids containing various forms of TFs (Fig. 1) were introduced to these cells using lipofectamin 2000 (Invitrogen) according to the manufacturer's recommendations. Cells were replated in Tc^+ or Tc^- media and selected for 2TS22C cells using 10 μg/ml blasticidin S (Invivogen) for 14 days or for ZHBTc4 cells using 1 μg/ml puromycin (Invivogen) for 10 days. Colonies identified by Leishman (Sigma, St Louis, MO) staining were counted. The rescue index of a given cDNA was determined by the ratio of colonies in Tc^+ to those in Tc^- media after subtracting the ratio of empty vector (background), which was then normalized by the ratio of *Sox2* or *Oct3/4* expression vector (positive control).

3. Results

3.1. PTDs interfere with the function of Sox2 and Oct3/4

To investigate whether Sox2 fused with PTD retained its normal function, we employed a functional complementation system based on the drug-inducible Sox2 knockout ES cells, 2TS22C. Here, endogenous *Sox2* is repressed in 2TS22C upon addition of Tc, which leads to differentiation of these cells and to reduction in colony-forming capacity (reflected in colony number). The number of

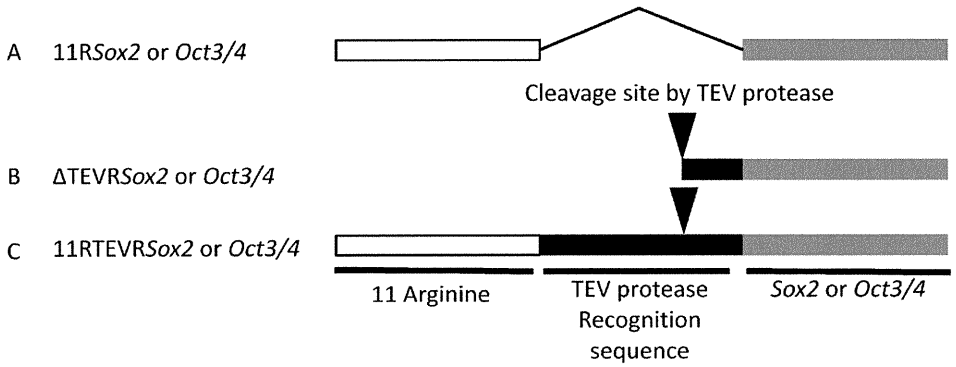

Fig. 1. Expression vectors used in the rescue experiments. (A) An eleven arginine (11R) sequence codon was ligated with *Sox2* or *Oct3/4* cDNA, (B) the residual sequence after cleavage of TEV protease was ligated with *Sox2* or *Oct3/4* cDNA, and (C) a TEV protease recognition sequence was inserted between the 11R sequence and *Sox2* or *Oct3/4* cDNA.

colonies increases only when exogenously introduced *Sox2* is functional (Masui et al., 2007). The normalized ratio of colony number, termed rescue index, reflects the relative activity of exogenous *Sox2*. When 11R or VP22 as a PTD was fused with Sox2, the rescue indices were greatly reduced compared with wild-type Sox2, suggesting that PTD interfered with the function of Sox2 (Table 1). Conversely, Sox2 fused with the residual sequence of the TEV protease recognition site showed an enhanced rescue index, suggesting that cleavage between PTD and Sox2 by TEV protease will be able to restore the function.

Next, to examine whether PTD disturbs the function of another TF, we assayed Oct3/4 fused with PTD in ZHBTc4, which represses endogenous *Oct3/4* expression in Tc^+ and loses colony-forming capacity. As in the case of Sox2, Oct3/4 fusion with 11R greatly reduced its function, whereas in the case of Oct3/4 without 11R (with the residual sequence of the TEV protease recognition site), the function was restored substantially (Table 1). These results suggest that the addition of PTD to TFs compromises the function of TFs, whereas intracellular removal of PTD by TEV protease restores the function.

3.2. Expression of TEV protease in ES cells does not compromise pluripotent stem cell specific gene expression

Wild-type TEV protease is known to be unstable because of its self-cleaving activity. More stable and efficient TEV protease mutants have been developed (Kapust et al., 2001), which are reported to be active in a variety of species including *E. coli* (Kapust and Waugh, 2000), yeast (Rigaut et al., 1999), *Drosophila* (Pauli et al., 2008), *Xenopus* (Wawersik et al., 2005) and rat (Wehr et al., 2006). To establish mouse ES cells expressing TEV protease, we infected mouse ES cells (2TS22C or ZHBTc4) with retroviruses carrying three types of TEV protease mutant (TEV-S219D, TEV-S219P or TEV-S219V). We confirmed that these ES cells expressed transgenes for TEV protease mutants (Fig. 2A). We then checked for the expression level of *Nanog*, marker gene for pluripotency, and found that they were maintained at almost the same level as the wild-type (Fig. 2B), suggesting that TEV protease did not cleave endogenous proteins necessary to maintain cellular identity.

Table 1
PTDs interfere with TF function.

Vectors	Tc^+ (Sox2 null)	Tc^-	Rescue index
(A) 2TS22C			
pPyCAGIB	22	344	0
pPyCAGSox2IB	270	286	1.0
pPyCAGIB/VP22Sox2	49	466	0.07
pPyCAGIB/11RSox2	57	436	0.09
pPyCAGIB/Δ TEVR-Sox2	162	258	0.63
Vectors	Tc^+ (Oct3/4 null)	Tc^-	Rescue index
(B) ZHBTc4			
pPyCAGIP	3	603	0
pPyCAGOct3/4IP	256	285	1.0
pPyCAGIP/11ROct3/4	8	216	0.03
pPyCAGIP/Δ TEVR-Oct3/4	248	298	0.93

The results of assay in 2TS22C (A) and ZHBTc4 (B). Colony numbers are shown in Tc^+ and Tc^- column.

3.3. TEV protease-expressing ES cells can restore the function of Sox2 fused with PTD

To address whether TEV protease can function in ES cells and contribute to restoring the function of TF by removing PTD, we introduced 11RSox2, ΔTEVRSox2, or 11RTEVRSox2 (containing TEV protease recognition site between 11R and Sox2) into wild-type 2TS22C or 2TS22C expressing the TEV protease mutants (2TS22C-TEVS219D, 2TS22C-TEVS219P or 2TS22C-TEVS219V). As

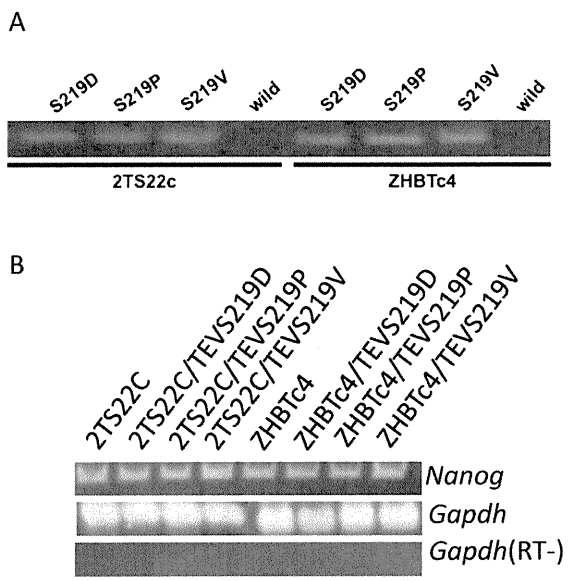

Fig. 2. Expression of TEV protease in ES cells does not compromise pluripotent stem cell specific gene expression. (A) RT-PCR analysis to confirm expression of transgenes for TEV protease mutants (S219D, S219P, S219V) and (B) RT-PCR analysis for *Nanog* in the ES cells.

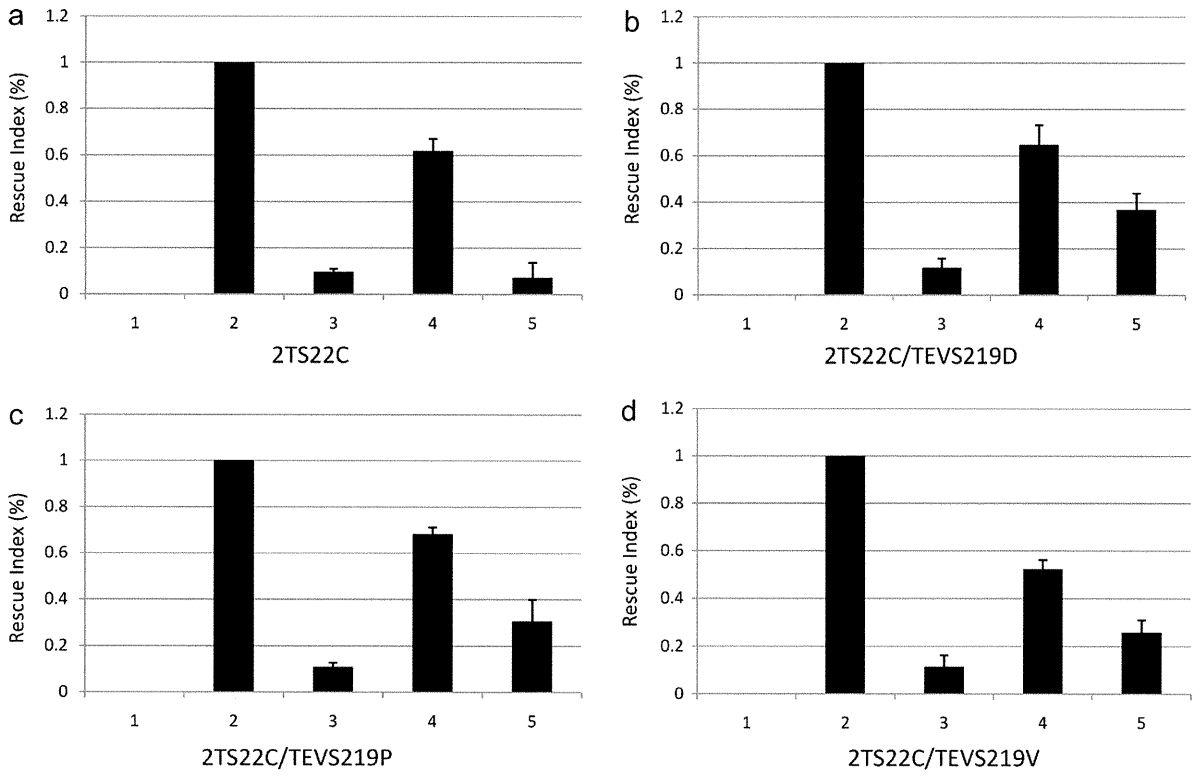

Fig. 3. TEV protease-expressing ES cells can restore the function of Sox2 fused with PTD. 1, pPyCAG-IB, empty vector; 2, pPyCAGSox2-IB; 3, pPyCAG-IB/11RSox2, 11R-containing Sox2; 4, pPyCAG-IB/ΔTEVRSox2, truncated form of Sox2 with residual fusion protein; 5, pPyCAG-IB/11RTEVRSox2, 11R-TEV recognition sequence-Sox2.

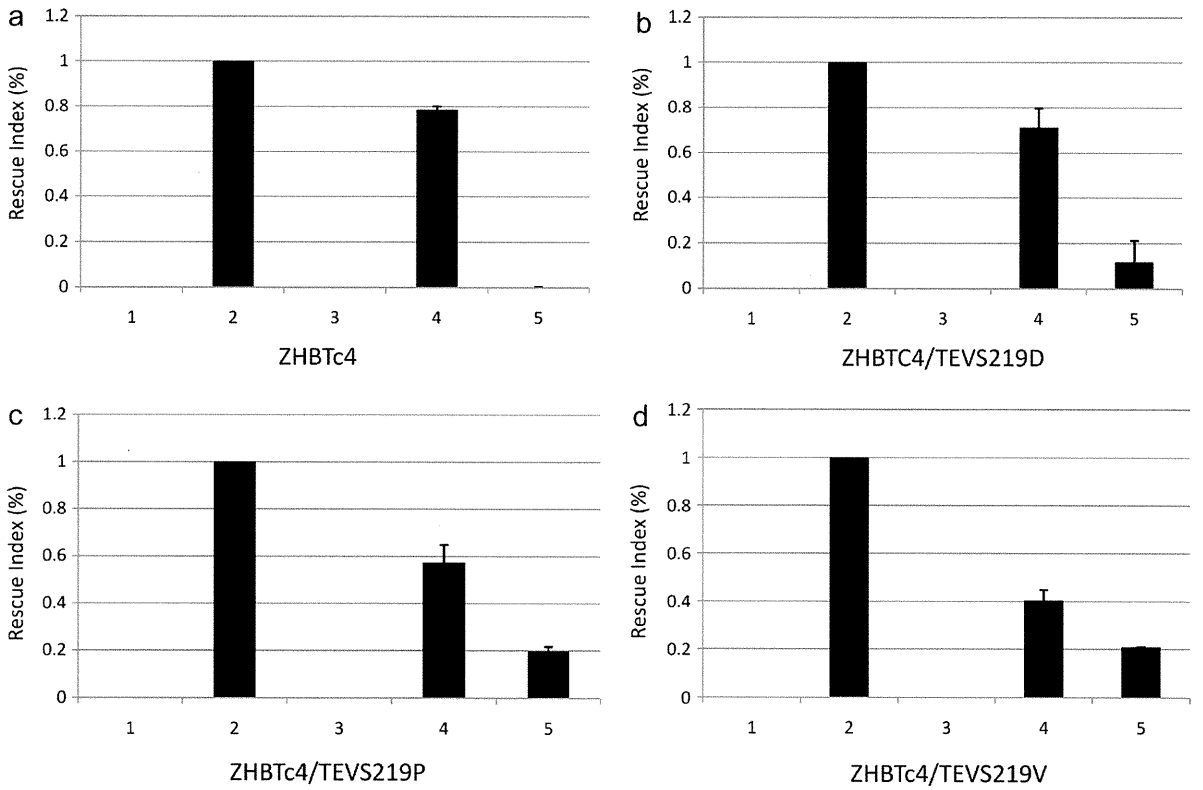

Fig. 4. TEV protease-expressing ES cells can restore the function of Oct3/4 fused with PTD. 1, pPyCAG-IP, empty vector; 2, pPyCAGOct3/4-IP; 3, pPyCAG-IP/11ROct3/4, 11R-containing Oct3/4; 4, pPyCAG-IP/ΔTEVROct3/4, truncated form of Oct3/4 with residual fusion protein; 5, pPyCAG-IP/11RTEVROct3/4, 11R-TEV recognition sequence-Oct3/4.

expected, the rescue index of 11RSox2 was greatly reduced (Fig. 3a–d, lane 3). In contrast, 11RTEVRSox2 substantially enhanced rescue index to a level comparable to that of ΔTEVRSox2 (Fig. 3b–d, lanes 4 and 5). This restoration of function was due to the activity of TEV protease, since no enhancement was observed in 2TS22C without the TEV protease transgene (Fig. 3a, lanes 4 and 5). These results indicate that the TEV protease cleaved 11RTEVRSox2 protein to remove PTD, which restored Sox2 function. The efficacy of the three TEV protease mutants was comparable.

3.4. TEV protease-expressing ES cells can restore the function of Oct3/4 fused with PTD

To determine whether the function of another TF can be recovered by removing the PTD, we introduced 11ROct3/4, ΔTEVROct3/4 or 11RTEVROct3/4 into wild-type ZHBTc4 or ZHBTc4 expressing the TEV protease mutants (ZHBTc4-TEVS219D, ZHBTc4-TEVS219P and ZHBTc4-TEVS219V). As expected, the rescue index of 11ROct3/4 was greatly reduced (Fig. 4a–d, lane 3). In contrast, 11RTEVROct3/4 substantially enhanced the rescue index to a level comparable to that of ΔTEVROct3/4 (Fig. 4b–d, lanes 4 and 5). This functional restoration was due to the activity of TEV protease, as no enhancement was observed in ZHBTc4 without the TEV protease transgene (Fig. 4a, lanes 4 and 5). These results indicate that TEV protease cleaved 11RTEVROct3/4 protein to remove PTD, which restored Oct3/4 function. The efficacy of the three TEV protease mutants was comparable.

Collectively, these results suggest that a PTD interferes with the function of TFs, which can be restored by intracellular removal of PTD by TEV protease.

4. Discussion

To date, there are three approaches to circumvent insertional mutagenesis in cellular induction experiments. (i) In a non-integration type DNA-based approach such as an episomal vector, occasional integration into the genome has been observed (Okita et al., 2008). Thus it is desirable to avoid introducing exogenous DNA into the cell. (ii) In an RNA-based approach, such as mRNA transfection (Warren et al., 2010), expression level may not be strong and continuous enough to induce global change in transcriptional profile. This may limit usefulness to general applications. In fact, a number of mRNA transfections are required for induction of iPS cells (Warren et al., 2010). Conversely, in Sendai virus (SeV), the RNA virus that does not integrate with the genome, transgene expression is known to be strong and continuous because SeV replicates in the cell (Li et al., 2000). Although it is known that SeV in the cells can be eliminated by using temperature-sensitive replication mutants of SeV (Inoue et al., 2003), for clinical use it will be difficult to achieve complete elimination from all the cells. This may result in unexpected effects of transgene TFs a long time after cell replacement therapy. (iii) A protein-based approach such as protein transduction, does not produce residual exogenous TFs upon withdrawal from the medium. In addition, unlike mRNA transfection, protein transduction does not require a transfection reagent, which is generally toxic to cells, so that TFs can be continuously added to the medium at a high concentration, enabling strong and continuous expression. However, their use has been hampered by the interference of PTDs with the function of TFs (Ye et al., 2002). In this study, we demonstrated that intracellular removal of PTD indeed restored the function of TFs using TEV protease as an example of this strategy. The activity of TEV protease was probably sufficient for processing most TFs, since quite a high level of exogenous Sox2 or Oct3/4 is known to be required for rescuing the repression of endogenous counterparts in ES cells. In future, it is conceivable that combination of PTD-TEVR-TFs introduced by protein transduction with TEV protease expressed by an RNA-based system (e.g., SeV) may achieve efficient cellular induction. In addition, this may reduce concern for any unexpected effect of expression of residual TFs (compared with all TFs being introduced by SeV), and may considerably reduce safety verification steps for clinical use.

In summary, we demonstrated that removal of PTD fused with Sox2 or Oct3/4 within ES cells restored protein function. This suggests that if PTD is removed from cells, directly delivered TF proteins, in general, may be able to exert substantially enhanced function than presently considered. This may enable induction of most cell types by protein transduction, and TEV protease may be a useful tool for this approach.

Funding

This work was supported in part by Grants-in-Aid for Scientific Research from the Ministry of Health, Labor, and Welfare of Japan.

Acknowledgments

We are grateful to Dr. Barbara Lee Smith Pierce (University of Maryland University College) for editorial work in the preparation of this manuscript.

References

Davis, R.L., Weintraub, H., Lassar, A.B., 1987. Expression of a single transfected cDNA converts fibroblasts to myoblasts. Cell 51, 987–1000.
Derossi, D., Calvet, S., Trembleau, A., Brunissen, A., Chassaing, G., Prochiantz, A., 1996. Cell internalization of the third helix of the Antennapedia homeodomain is receptor-independent. J. Biol. Chem. 271, 18188–18193.
Dougherty, W.G., Carrington, J.C., Cary, S.M., Parks, T.D., 1988. Biochemical and mutational analysis of a plant virus polyprotein cleavage site. EMBO J. 7, 1281–1287.
Feng, R., Desbordes, S.C., Xie, H., Tillo, E.S., Pixley, F., Stanley, E.R., Graf, T., 2008. PU.1 and C/EBPalpha/beta convert fibroblasts into macrophage-like cells. Proc. Natl. Acad. Sci. U.S.A. 105, 6057–6062.
Frankel, A.D., Pabo, C.O., 1988. Cellular uptake of the tat protein from human immunodeficiency virus. Cell 55, 1189–1193.
Hanna, J., Wernig, M., Markoulaki, S., Sun, C.W., Meissner, A., Cassady, J.P., Beard, C., Brambrink, T., Wu, L.C., Townes, T.M., Jaenisch, R., 2007. Treatment of sickle cell anemia mouse model with iPS cells generated from autologous skin. Science 318, 1920–1923.
Ieda, M., Fu, J.D., Delgado-Olguin, P., Vedantham, V., Hayashi, Y., Bruneau, B.G., Srivastava, D., 2010. Direct reprogramming of fibroblasts into functional cardiomyocytes by defined factors. Cell 142, 375–386.
Inoue, M., Tokusumi, Y., Ban, H., Kanaya, T., Tokusumi, T., Nagai, Y., Iida, A., Hasegawa, M., 2003. Nontransmissible virus-like particle formation by F-deficient sendai virus is temperature sensitive and reduced by mutations in M and HN proteins. J. Virol. 77, 3238–3246.
Kapust, R.B., Tozser, J., Fox, J.D., Anderson, D.E., Cherry, S., Copeland, T.D., Waugh, D.S., 2001. Tobacco etch virus protease: mechanism of autolysis and rational design of stable mutants with wild-type catalytic proficiency. Protein Eng 14, 993–1000.
Kapust, R.B., Waugh, D.S., 2000. Controlled intracellular processing of fusion proteins by TEV protease. Protein Expr Purif 19, 312–318.
Kim, D., Kim, C.H., Moon, J.I., Chung, Y.G., Chang, M.Y., Han, B.S., Ko, S., Yang, E., Cha, K.Y., Lanza, R., Kim, K.S., 2009. Generation of human induced pluripotent stem cells by direct delivery of reprogramming proteins. Cell Stem Cell 4, 472–476.
Li, H.O., Zhu, Y.F., Asakawa, M., Kuma, H., Hirata, T., Ueda, Y., Lee, Y.S., Fukumura, M., Iida, A., Kato, A., Nagai, Y., Hasegawa, M., 2000. A cytoplasmic RNA vector derived from nontransmissible Sendai virus with efficient gene transfer and expression. J. Virol. 74, 6564–6569.
Masui, S., Nakatake, Y., Toyooka, Y., Shimosato, D., Yagi, R., Takahashi, K., Okochi, H., Okuda, A., Matoba, R., Sharov, A.A., Ko, M.S., Niwa, H., 2007. Pluripotency governed by Sox2 via regulation of Oct3/4 expression in mouse embryonic stem cells. Nat. Cell Biol. 9, 625–635.
Matsushita, M., Tomizawa, K., Moriwaki, A., Li, S.T., Terada, H., Matsui, H., 2001. A high-efficiency protein transduction system demonstrating the role of PKA in long-lasting long-term potentiation. J. Neurosci. 21, 6000–6007.
Morita, S., Kojima, T., Kitamura, T., 2000. Plat-E: an efficient and stable system for transient packaging of retroviruses. Gene Ther. 7, 1063–1066.
Niwa, H., Miyazaki, J., Smith, A.G., 2000. Quantitative expression of Oct-3/4 defines differentiation, dedifferentiation or self-renewal of ES cells. Nat. Genet. 24, 372–376.
Okita, K., Ichisaka, T., Yamanaka, S., 2007. Generation of germline-competent induced pluripotent stem cells. Nature 448, 313–317.

Okita, K., Nakagawa, M., Hyenjong, H., Ichisaka, T., Yamanaka, S., 2008. Generation of mouse induced pluripotent stem cells without viral vectors. Science 322, 949–953.

Pauli, A., Althoff, F., Oliveira, R.A., Heidmann, S., Schuldiner, O., Lehner, C.F., Dickson, B.J., Nasmyth, K., 2008. Cell-type-specific TEV protease cleavage reveals cohesin functions in Drosophila neurons. Dev Cell 14, 239–251.

Phelan, A., Elliott, G., O'Hare, P., 1998. Intercellular delivery of functional p53 by the herpesvirus protein VP22. Nat. Biotechnol. 16, 440–443.

Rigaut, G., Shevchenko, A., Rutz, B., Wilm, M., Mann, M., Seraphin, B., 1999. A generic protein purification method for protein complex characterization and proteome exploration. Nat Biotechnol 17, 1030–1032.

Takahashi, K., Yamanaka, S., 2006. Induction of pluripotent stem cells from mouse embryonic and adult fibroblast cultures by defined factors. Cell 126, 663–676.

Takenobu, T., Tomizawa, K., Matsushita, M., Li, S.T., Moriwaki, A., Lu, Y.F., Matsui, H., 2002. Development of p53 protein transduction therapy using membrane-permeable peptides and the application to oral cancer cells. Mol. Cancer Ther. 1, 1043–1049.

Vierbuchen, T., Ostermeier, A., Pang, Z.P., Kokubu, Y., Sudhof, T.C., Wernig, M., 2010. Direct conversion of fibroblasts to functional neurons by defined factors. Nature 463, 1035–1041.

Warren, L., Manos, P.D., Ahfeldt, T., Loh, Y.H., Li, H., Lau, F., Ebina, W., Mandal, P.K., Smith, Z.D., Meissner, A., Daley, G.Q., Brack, A.S., Collins, J.J., Cowan, C., Schlaeger, T.M., Rossi, D.J., 2010. Highly efficient reprogramming to pluripotency and directed differentiation of human cells with synthetic modified mRNA. Cell Stem Cell 7, 618–630.

Wawersik, S., Evola, C., Whitman, M., 2005. Conditional BMP inhibition in Xenopus reveals stage-specific roles for BMPs in neural and neural crest induction. Dev Biol 277, 425–442.

Wender, P.A., Mitchell, D.J., Pattabiraman, K., Pelkey, E.T., Steinman, L., Rothbard, J.B., 2000. The design, synthesis, and evaluation of molecules that enable or enhance cellular uptake: peptoid molecular transporters. Proc. Natl. Acad. Sci. U.S.A. 97, 13003–13008.

Wernig, M., Zhao, J.P., Pruszak, J., Hedlund, E., Fu, D., Soldner, F., Broccoli, V., Constantine-Paton, M., Isacson, O., Jaenisch, R., 2008. Neurons derived from reprogrammed fibroblasts functionally integrate into the fetal brain and improve symptoms of rats with Parkinson's disease. Proc. Natl. Acad. Sci. U.S.A. 105, 5856–5861.

Wehr, M.C., Laage, R., Bolz, U., Fischer, T.M., Grunewald, S., Scheek, S., Bach, A., Nave, K.A., Rossner, M.J., 2006. Monitoring regulated protein-protein interactions using split TEV. Nat Methods 3, 985–993.

Ye, D., Xu, D., Singer, A.U., Juliano, R.L., 2002. Evaluation of strategies for the intracellular delivery of proteins. Pharm. Res. 19, 1302–1309.

Zhou, Q., Brown, J., Kanarek, A., Rajagopal, J., Melton, D.A., 2008. In vivo reprogramming of adult pancreatic exocrine cells to beta-cells. Nature 455, 627–632.